Mathematical Models and Methods in Applied Sciences
Vol. 27, No. 1 (2017) 205–230

DOI: 10.1142/S0218202517400073

Efficient numerical methods for multiscale crowd dynamics with emotional contagion

Li Wang

Department of Mathematics, Computational and Data-Enabled Science and Engineering Program, State University of New York at Buffalo, 244 Mathematics Building, Buffalo, NY 14260, USA
lwang46@buffalo.edu

Martin B. Short

Department of Mathematics, Georgia Institute of Technology, 686 Cherry Street, Atlanta, GA 30332-0160, USA
mbshort@math.gatech.edu

Andrea L. Bertozzi

Department of Mathematics, University of California, Los Angeles, 520 Portola Plaza, Los Angeles, CA 90095, USA
bertozzi@math.ucla.edu

Received 13 May 2016
Revised 21 September 2016
Accepted 1 October 2016
Published 30 December 2016
Communicated by N. Bellomo, F. Brezzi and M. Pulvirenti

In this paper, we develop two efficient numerical methods for a multiscale kinetic equation in the context of crowd dynamics with emotional contagion [A. Bertozzi, J. Rosado, M. Short and L. Wang, Contagion shocks in one dimension, *J. Stat. Phys.* **158** (2014) 647–664]. In the continuum limit, the mesoscopic kinetic equation produces a natural Eulerian limit with nonlocal interactions. However, such limit ceases to be valid when the underlying microscopic particle characteristics cross, corresponding to the blow up of the solution in the Eulerian system. One method is to couple these two situations — using Eulerian dynamics for regions without characteristic crossing and kinetic evolution for regions with characteristic crossing. For such a hybrid setting, we provide a regime indicator based on the macroscopic density and fear level, and propose an interface condition via continuity to connect these two regimes. The other method is based on a level set formulation for the continuum system. The level set equation shares similar forms as the kinetic equation, and it successfully captures the multi-valued solution in velocity, which implies that the multi-valued solution other than the viscosity solution should be the physically relevant ones for the continuum system. Numerical examples are presented to show the efficiency of these new methods.

Keywords: Crowd dynamics; hybrid scheme; level set method; multi-valued solution.

AMS Subject Classification: 35Q82, 35L65, 65M08

1. Introduction

Multiscale phenomena find applications in a broad range of scientific problems such as gases out of thermodynamic equilibrium, turbulence in fluids, and radiative transfer with variational collision rate. In most of these situations, the majority of the domain can be characterized by the macroscopic model, except in some small regions where microscopic effects are important such as near the boundaries or shock layers. Moreover, the macroscopic model gives the most efficient description, as it resides in physical space and requires the lowest computational cost; compare this to the mesoscopic kinetic model that resides in phase space, and the microscopic model that records the evolution of each individual. Therefore, it is desirable to use the macroscopic model whenever possible, and to restrict the use of the kinetic model to only those locations where it is necessary.

To this aim, domain decomposition technology has been widely explored, especially in the context of neutron transport with a macroscopic diffusion limit,[29,28,3,53] the Boltzmann equation with an Eulerian or Navier–Stokes limit,[11,40,39] and the hyperbolic relaxation system with multiple relaxation times.[37,19] At the same time, a hybrid scheme has gained popularity in multiscale kinetic equations as well for its automatic detection of different regimes; consult Refs. 24, 20, 21 and 27 for a recent extension to better regime indicator and higher-order coupling.

One particular domain in which both continuum and kinetic models are often employed is the dynamics of human crowds. Due to the complexity of human crowd behavior, mathematical modeling of their motion has attracted a lot of attention, and the literature is large (see Refs. 5 and 34). In broad terms, the models that have been proposed can be grouped into two classes by scales. One class is the microscopic, individual-based model inspired by Newtonian mechanics focusing on inter-particle interaction, often referred to as "social force" models. There, each person is treated as a particle experiencing a simple, intuitive interaction to adapt its walking speed and direction.[30,32] The other class treats the crowd as a continuum flow, which is well suited for large-scale, dense crowds provided the characteristic length between pedestrians is much less than the typical length scale of the region. These continuum models are typically derived either from microscopic discrete models via kinetic theory or directly following a fluid dynamic approach with fluxes from optimal control theory or mean-field games.[1,25,2]

In this paper, we focus on a particular multiscale crowd model known as ASCRIBE.[8] This model has the interesting property of tracking the level of fear within the individual agents, which is assumed to influence their motion and also exhibits contagion-like properties, described in detail below. This model has been used in the agent-based simulation tool ESCAPES[55] that has been used to model evacuation scenarios of the International Terminal at Los Angeles International Airport (LAX). It has also been found that the ASCRIBE model has compared favorably to actual crowd footage relative to other crowd models.[54]

In Ref. 7, a mathematical look at the ASCRIBE model through particle, continuum, and kinetic descriptions was developed. In this model, the kinetic description

in one dimension takes the form

$$f_t + (qf)_x = \gamma((q - q^*)f)_q, \tag{1.1}$$

where $f(t, x, q)$ is the probability of finding a person with fear level q at time t and position x. The quantity $q^*(t, x)$ is the local "average" fear level weighted by the distance to x:

$$q^*(t, x) = \frac{\iint \kappa(|x - y|)f(t, y, q)qdqdy}{\iint \kappa(|x - y|)f(t, y, q)dqdy}.$$

It models the fact that people's emotion will be affected by their neighborhood. Here $\kappa(r)$ is the interaction kernel that decays with r and integrates to one. The continuum limit of (1.1) is obtained by taking the zeroth and first moment of (1.1). That is, multiplying (1.1) by $(1, q)^T$ and integrating against q, one has

$$\rho_t + (\rho\tilde{q})_x = 0, \quad (\rho\tilde{q})_t + (\rho\tilde{q}^2)_x = \gamma\rho(q^* - \tilde{q}) \tag{1.2}$$

under the mono-kinetic distribution assumption (which will be specified in the next section). Here $\rho(t, x)$ and $\tilde{q}(t, x)$ are the macroscopic density and bulk fear level:

$$\rho(t, x) = \int f(t, x, q)dq, \quad \rho\tilde{q}(t, x) = \int f(t, x, q)qdq. \tag{1.3}$$

The continuum equation (1.2) can be considered as a pressureless Euler equation augmented with a nonlocal alignment which acts as a regularization. It has been shown in Refs. 7 and 51 that there exists a critical threshold depending on the equilibration rate γ and radius of interaction, such that if the initial variation of the fear level $\partial_x q(0, x)$ is above the threshold the system admits a global smooth solution. Such a solution will lead to a flocking in the long time limit for if we further assume the initial data is compactly supported.[51,14] Let us mention that the critical threshold phenomenon is typical for nonlocal PDE, see for example Ref. 45 for a scalar conservation law. On the other hand, if the initial variation is below the threshold, there is a finite time break down of the continuum system (q_x and ρ blow up) and shock forms in q. This, in analogy with the microscopic agent-based model, means the particle characteristics cross. In this case, the continuum model fails and the kinetic model is necessary. Therefore, this crowd contagion dynamics has displayed a multiscale structure: when the underlying microscopic particle characteristics do not cross, a continuum description is enough, otherwise a kinetic model is needed.

To efficiently simulate such multiscale dynamics, we develop here a hybrid method where a kinetic solver is switched on wherever the macroscopic description ceases to be valid. The microscopic and macroscopic variables are linked through the local equilibrium. However, unlike the Boltzmann equation in the hydrodynamic regime whose local equilibrium is a well-defined Maxwellian, the equilibrium here is a delta function in the velocity space, which makes any regime indicator that depends on it very sensitive to the way the delta function is approximated. To this end, we propose a *uniform* indicator that works for both transitions from kinetic to continuum and vice versa. It depends on the distance of $\tilde{q}$ and q^* following an

asymptotic property of (1.1). A threshold on the magnitude of ρ is also placed to avoid mislabeling near the center of the shock.

Now let us consider the problem from a different point of view. Notice that the failure of the continuum system lies in the blow up of density, which comes from the formation of a shock in fear. However, in real situation, people who are more scared will pass through the less scared ones ahead of them, and lead to a mixed case where people with different fear levels may be present at the same position. Therefore it is desirable to consider *multi-valued* fear solution instead of the shock solution. This is also suggested by the microscopic particles system, as crossing of particle characteristics leads to a multi-valued fear level. The study of numerical methods for computing multi-valued solutions is pervasive in different contexts, such as Refs. 38, 35, 47, 17, 18 and references therein. The methods basically fall into two categories: one is a particle method and the other is a level set method. The particle method is easy to implement and free of numerical dissipation, but designing a robust recovery method of the point values from its particle approximation is a challenging task, and the computational cost is sometimes very high (in our case it is $O(N^2)$ with N being the number of particles). Here we take the level set approach, and formulate a level set equation for computing the multi-valued fear level. To compute the density, we derive another evolution equation based on a new function, which follows the same spirit as in Ref. 36. This level set equation is of similar form as the kinetic equation, but a local level set method can be utilized to significantly reduce the computational cost in phase space.

The rest of the paper is organized as follows. In Sec. 2, we give a brief review of the contagion dynamics and provide a simple derivation to link the different levels of model hierarchy. Section 3 is devoted to the hybrid algorithms and contains the regime indicator, interface condition, and discretization. In Sec. 4, we develop a level set formulation for the continuum system, and in Sec. 5, we present several numerical examples to show the performance of these two schemes. Finally, the paper is concluded in Sec. 6.

2. Contagion Dynamics with Continuum Limit

In this section, we briefly review the contagion dynamics in one dimension, and provide a formal relationship between different levels of the models. First, the agent-based model in the microscopic level reads

$$\frac{dx_i}{dt} = q_i, \quad \frac{dq_i}{dt} = \gamma(q_i^* - q_i), \quad q_i^* = \frac{\sum_{j=1}^N \kappa_{i,j} q_j}{\sum_{j=1}^N \kappa_{i,j}}, \quad i = 1, 2, \ldots, N, \tag{2.1}$$

where each particle i represents a person, and $x_i(t)$ and $q_i(t)$ are its position and fear level. Here we assume that velocity is proportional to fear level, which simply means that agents will run faster if more scared; this assumption has been made by others.[4,6] The fear q_i, meanwhile, undergoes a form of contagion, whereby agents tend to equilibrate their own fear level with a weighted average of the fear level of

the other agents, q_i^*. Because of this dynamic, the range of fear levels exhibited by the various agents is bounded between whatever the minimum and maximum fear levels were at $t = 0$. The interaction kernel $\kappa_{i,j} = \kappa(|x_i - x_j|)$, which serves as the weights in the average q_i^*, is a decreasing function of mutual distance between two particles and is parametrized by an interaction distance R. N is the total number of particles. Parameter γ describes the contagion interaction strength and it may vary with particle for more general cases.

The microscopic system (2.1) is often too expensive to compute as N becomes large, in which case one needs to consider the next level of the model — the kinetic level. The passage from the microscopic system to kinetic description can be accomplished via a mean-field limit.[15,12] Denote the empirical distribution density by

$$f^N = \frac{1}{N}\sum_{i=1}^{N} \delta(x - x_i(t))\delta(q - q_i(t)), \tag{2.2}$$

where δ is Dirac delta function, and we assume that the particles remain in a fixed compact domain $(x_i(t), q_i(t)) \in \Omega \subset \mathbb{R}^2$ for all i and up to the time we consider. Then Prohorov's theorem implies that the sequence $\{f^N\}$ is weakly$*$ relatively compact. Therefore, there exists a subsequence $\{f^{N_k}\}_k$ such that f^{N_k} converges to f with $weak^*$-convergence in $\mathcal{P}(\mathbb{R}^2)$ and pointwisely in time as $k \to \infty$. Here $\mathcal{P}(\mathbb{R}^2)$ denotes the space of probability measure on $\mathbb{R}^2$. Now consider a test function $\psi \in C_0^1(\mathbb{R}^2)$, we have

$$\begin{aligned}
\frac{d}{dt}\langle f^N, \psi\rangle_{x,q} &= \frac{d}{dt}\left\langle \frac{1}{N}\sum_{i=1}^{N} \delta(x - x_i(t))\delta(q - q_i(t)), \psi \right\rangle_{x,q} \\
&= \frac{d}{dt}\frac{1}{N}\sum_{i=1}^{N} \psi(x_i(t), q_i(t)) \\
&= \frac{1}{N}\sum_{i=1}^{N} \psi_x q_i + \psi_q \gamma(q_i^* - q_i) \\
&= \langle \psi_x q, f^N\rangle + \frac{\gamma}{N}\sum_{i=1}^{N} \psi_q \left(\frac{\sum_{j=1}^{N} \kappa_{i,j} q_j}{\sum_{j=1}^{N} \kappa_{i,j}} - q_i\right).
\end{aligned} \tag{2.3}$$

Here $\langle \bullet \rangle_{x,q}$ means integration against both x and q, and $\langle \bullet \rangle_x$ means integration only in x. Further,

$$\frac{1}{N}\sum_{j=1}^{N} \kappa(|x_i - x_j|) = \left\langle \kappa(|x_i - y|), \frac{1}{N}\sum_{j=1}^{N} \delta(y - x_j) \right\rangle_x = \kappa * \rho_{f^N}(x_i),$$

$$\frac{1}{N}\sum_{j=1}^{N} \kappa(|x_i - x_j|) q_j = \left\langle \kappa(|x_i - y|), \frac{1}{N}\sum_{j=1}^{N} \delta(y - x_j) q_j \right\rangle_x = \kappa * m_{f^N}(x_i),$$

where we have used the definitions

$$\rho_{f^N}(x) = \frac{1}{N}\sum_{i=1}^{N}\delta(x - x_i)$$

and

$$m_{f^N}(x) = \left\langle q, \frac{1}{N}\sum_{j=1}^{N}\delta(x - x_j)\delta(q - q_j)\right\rangle_{x,q} = \frac{1}{N}\sum_{j=1}^{N}\delta(x - x_j)q_j.$$

Therefore (2.3) reads

$$\frac{d}{dt}\langle f^N, \psi\rangle_{x,q} = \langle \psi_x q, f^N\rangle_{x,q} + \gamma\left\langle f^N, \frac{\kappa * m_{f^N}}{\kappa * \rho_{f^N}}\psi_q - q\psi_q\right\rangle_{x,q},$$

which leads to

$$f^N_t + (qf^N)_x = \gamma((q - q^*)f^N)_q, \quad q^* = \frac{\iint \kappa(|x - y|)f(y, q)qdqdy}{\iint \kappa(|x - y|)f(y, q)dqdy} \tag{2.4}$$

via integration by parts. Now letting $k \to \infty$, the subsequence f^{N_k} formally leads to the limiting kinetic equation

$$f_t + (qf)_x = \gamma((q - q^*)f)_q. \tag{2.5}$$

Third, we derive its continuum limit. Take the moments of (2.5), we have the following evolution equations for the macroscopic quantities: the mass density $\rho(t, x)$ and bulk fear level $\tilde{q}(t, x)$ defined in (1.3):

$$\rho_t + (\rho\tilde{q})_x = 0, \quad (\rho\tilde{q})_t + (\rho\tilde{q}^2 + P)_x = \gamma\rho(q^* - \tilde{q}), \tag{2.6}$$

where the pressure $P(t, x)$ given by

$$P(t, x) = \int (q - \tilde{q})^2 f(t, x, q)dq. \tag{2.7}$$

Now we assume that the particle distribution is mono-kinetic in velocity space, i.e.

$$f(t, x, q) = \rho(t, x)\delta(q - \tilde{q}(t, x)), \tag{2.8}$$

then the pressure vanishes and (2.6) is rewritten as

$$\begin{cases} \rho_t + (\rho\tilde{q})_x = 0, \\ (\rho\tilde{q})_t + (\rho\tilde{q}^2)_x = \gamma\rho(q^* - \tilde{q}), \quad q^* = \dfrac{\int \kappa(|x - y|)\rho(y)\tilde{q}(y)dy}{\int \kappa(|x - y|)\rho(y)dy}, \end{cases} \tag{2.9}$$

which can be considered as a pressureless Euler equation with a nonlocal alignment. Note that, at least formally, system (2.9) reduces to the classical pressureless Euler system[13,9] in the limit of zero interaction radius and infinite interaction rate, i.e. $\gamma \to \infty$ and $R \to 0$. Such system arises in modeling sticky particles in gas dynamics, and its solution admits a δ-shock that has been well-understood both analytically[33,16,9,43,44,50] and numerically.[10] Here in the second equation of (2.9), the nonlocal alignment can help to regularize the δ-singularity and may lead to a global

classical solution under some appropriate assumption.[7,51] When classical solution exists, the second equation in (2.9) is equivalent to the following non-conservative form:

$$\tilde{q}_t + \tilde{q}\tilde{q}_x = \gamma(q^* - \tilde{q}). \tag{2.10}$$

When classical solution does not globally exist, in which case q_x blows up in finite time (a shock in q forms), a kinetic model is needed after the break down of the continuum system. From a microscopic point of view, this case corresponds to the crossing of particles' characteristics.

To end this section, we would like to mention an interesting result in Ref. 46 for self-organized dynamics, whose model in one dimension is the same as ours. In that paper, the authors focus on the long-time behavior (or so-called flocking behavior) that characterizes a long-time "equilibrium" when all particles form into one cluster with the same speed. On the contrary, in this paper we are interested in the transient behavior, especially when the particle characteristics can cross, whose long-time behavior may not be flocking. Moreover, we would like to treat different kinds of initial data, not just those with compact support as is considered in Ref. 46 (in analogy with the agent-based model, compact support means a finite number of agents).

3. Hybrid Scheme Via Kinetic Formation

The high dimensionality makes the kinetic equation expensive to compute, while the continuum system breaks down in the presence of the crossing of characteristics. It is therefore desirable to construct a hybrid scheme that automatically becomes a kinetic solver whenever the particles in the underlying microscopic system tend to cross and stays as a macroscopic solver when particles are kept a certain distance away.

3.1. *Regime indicators*

Our first task is to provide a formal justification of the mono-kinetic distribution that links the kinetic equation (2.5) with continuum system (2.9). Consider a space homogeneous toy model

$$f_t = \frac{1}{\epsilon}[(q - q^*)f]_q, \quad \int_{\mathbb{R}} f(0,q)dq = 1, \tag{3.1}$$

where q^* is any *constant*. The following proposition highlights the relaxation of the kinetic solution f toward the mono-kinetic distribution (2.8) at the fast ϵ time scale.

Proposition 3.1. *Let $f(t,q) > 0$ be the solution to the initial value problem of the space homogeneous equation (3.1). Assume $f(t,q)$ decays faster than $\frac{1}{|q|^2}$ as $|q| \to \infty$. Then f converges to $\delta(q - \tilde{q}(t))$ and $\delta(q - q^*)$ formally as $\epsilon \to 0$, where $\tilde{q} = \int f(t,q)qdq$. Therefore, $\tilde{q}(t) \to q^*$.*

Proof. Denote the variance

$$\mathcal{F}(t) = \int_{\mathbb{R}} (q - \tilde{q}(t))^2 f(t,q) dq, \tag{3.2}$$

then

$$\frac{d\mathcal{F}}{dt} = \int_{\mathbb{R}} (q-\tilde{q})^2 f_t + 2(\tilde{q}-q)\tilde{q}_t f dq = \int_{\mathbb{R}} (q-\tilde{q})^2 f_t dq = \frac{1}{\epsilon}\int_{\mathbb{R}} (q-\tilde{q})^2 [(q-q^*)f]_q dq$$
$$= -\frac{2}{\epsilon}\int_{\mathbb{R}} (q-q^*)(q-\tilde{q}) f dq = -\frac{2}{\epsilon}\int_{\mathbb{R}} q(q-\tilde{q}) f dq,$$

here the second and last equalities use the fact that $\int_{\mathbb{R}} q f dq = \tilde{q}$, and the fourth one uses integration by parts. Notice that

$$\int_{\mathbb{R}} q^2 f dq - \int_{\mathbb{R}} q\tilde{q} f dq = \int_{\mathbb{R}} q^2 f dq \int_{\mathbb{R}} f dq - \left(\int_{\mathbb{R}} f q dq\right)^2 \geq 0,$$

thanks to the Cauchy–Schwarz inequality, we have $\frac{d\mathcal{F}}{dt} \leq 0$. As a matter of fact, we have

$$\frac{d\mathcal{F}}{dt} = -\frac{2}{\epsilon}\int_{\mathbb{R}} q(q-\tilde{q}) f dq = -\frac{2}{\epsilon}\int_{\mathbb{R}} (q-\tilde{q})^2 f dq = -\frac{2}{\epsilon}\mathcal{F},$$

thus $\mathcal{F} \to 0$ as $\epsilon \to 0$, and thus the equilibrium solution is $f = \delta(q - \tilde{q})$. Similarly, let $\mathcal{G}(t) = \int_{\mathbb{R}} (q-q^*)^2 f(t) dq$, then

$$\frac{d\mathcal{G}}{dt} = \int_{\mathbb{R}} (q-q^*)^2 f_t dq = \frac{1}{\epsilon}\int_{\mathbb{R}} (q-q^*)^2 [(q-q^*)f]_q dq$$
$$= -\frac{2}{\epsilon}\int_{\mathbb{R}} (q-q^*)^2 f dq = -\frac{2}{\epsilon}\mathcal{G}.$$

Hence f converges to $\delta(q-q^*)$, and together with the above result leads to $\tilde{q}(t) \to q^*$. □

Now we return to the space inhomogeneous case

$$f_t + q f_x = \frac{1}{\epsilon}[(q-q^*)f]_q, \tag{3.3}$$

where similar arguments can apply to show

Proposition 3.2. *Let $f(t,x,q) > 0$ be the solution to the initial value problem of the space inhomogeneous equation* (3.3)*. Assume $f(t,x,q)$ decays faster than $\frac{1}{|q|^2}$ as $|q| \to \infty$. Then as ϵ tends to* 0*, we formally have f converging to $\rho(t,x)\delta(q-q^*(t,x))$ and $\rho(t,x)\delta(q-\tilde{q}(t,x))$ with $\rho(t,x)$ and $\tilde{q}(t,x)$ defined in* (1.3) *and $q^*(t,x)$ defined in* (2.9)*.*

Proof. The proof is similar to that in Proposition 3.1. Again denote

$$\mathcal{F}(t,x) = \int_{\mathbb{R}} (q - \tilde{q}(t,x))^2 f(t,x,q) dq, \tag{3.4}$$

then

$$\begin{aligned}\frac{d\mathcal{F}}{dt} &= -\frac{2}{\epsilon}\int (q-\tilde{q})(q-q^*)f\,dq - \int q f_x (q-\tilde{q})^2 dq \\ &= -\frac{2}{\epsilon}\int (q-\tilde{q})^2 f\,dq - \int q f_x (q-\tilde{q})^2 dq \\ &= -\frac{2}{\epsilon}\mathcal{F} - \int q f_x (q-\tilde{q})^2 dq.\end{aligned}$$

Thus in the limit $\epsilon \to 0$, we have $\mathcal{F} = 0$. Therefore, the dependence of f on q converges to a delta function $\delta(q-\tilde{q}(t,x))$. Then by conservation of mass, we have $f \to \rho(t,x)\delta(q-\tilde{q}(t,x))$. The convergence of f toward $\rho(t,x)\delta(q-q^*(t,x))$ similarly follows. □

The above propositions provide insight on the situation wherein continuum system (2.9) is a good approximation to the kinetic model (2.5), that is, when γ is large enough. This is consistent with Theorem 4 in Ref. 7. Moreover, since $\tilde{q}$ approaches q^* at the same time when f converges to the mono-kinetic distribution, it suggests a mechanism to label the solutions in different regimes. That is, one can check

$$|\tilde{q}(t,x) - q^*(t,x)| > \epsilon_0 \tag{3.5}$$

for every x. If it holds, then this point falls into the kinetic regime, otherwise it is labeled as a continuum point. A reasonable choice of ϵ_0 is

$$\epsilon_0 = \max_x |q^*(0,x) - \tilde{q}(0,x)|. \tag{3.6}$$

Notice however, when the continuum model is no longer valid and $\tilde{q}(x)$ is very different from $q^*(x)$, there could still be $\tilde{q}(x) = q^*(x)$ at some points (such as their intersection). Therefore, to avoid mislabeling such points as continuum regime, we propose another criteria to accompany (3.5):

$$\rho(x) > \rho_{\max}. \tag{3.7}$$

This means that if the density is beyond a threshold, which in analogy with the agent-based model means two particles are too close, we need to switch on the kinetic solver. Here a rough choice of $\rho_{\max}$ is $\rho_{\max} = \max_x \rho(0,x)$, but more detailed ones are problem-dependent, and will be specified for each examples in Sec. 5. Since the indicator (3.5), (3.7) only depends on macroscopic quantities $\tilde{q}$, q^* and ρ, it will be used for both the transition from kinetic to continuum or continuum to kinetic regimes.

Remark 3.1. Since the mono-kinetic distribution $\rho(t,x)\delta(q-\tilde{q}(t,x))$ can be considered as a local equilibrium, a natural criteria from kinetic to continuum would be $\|f(t,x,q) - \rho(t,x)\delta(q-\tilde{q}(t,x))\|_q < \epsilon_1$ for some small constant ϵ_1. However, one can only approximate the δ-function, which makes such a measure very sensitive to the way we do the approximation. So, we will not use this criteria but stick to (3.5), (3.7) for both transitions.

3.2. *Space and velocity discretization*

In this section, we summarize numerical discretization of both kinetic equation (2.5) and continuum system (2.9), and postpone the interface condition to the next section. The choice of discretization is not unique, see for example, Refs. 49 and 52, and most shock capturing methods for hyperbolic systems will apply.

Divide the spatial and velocity domain into a number of cells $[x_{j-\frac{1}{2}}, x_{j+\frac{1}{2}}]$ and $[q_{k-\frac{1}{2}}, q_{k+\frac{1}{2}}]$, where $j \in 1, 2, \ldots, N_x,\ k \in 1, 2, \ldots, N_q$. Here N_x and N_q are the total number of points in x- and q-directions, respectively. Each cell is centered at x_j or q_k with a uniform length Δx and Δq. Denote $f_{j,k} = f(t, x_j, q_k)$ and $q_j^* = q^*(t, x_j)$, then a first-order semi-discrete upwind scheme of the kinetic equation (2.5) reads

$$\partial_t f_{j,k} + \frac{\eta_{j+\frac{1}{2},k} - \eta_{j-\frac{1}{2},k}}{\Delta x} + \gamma \frac{\xi_{j,k+\frac{1}{2}} - \xi_{j,k-\frac{1}{2}}}{\Delta q} = 0, \tag{3.8}$$

where

$$\begin{aligned} \eta_{j+\frac{1}{2},k} &= \frac{|q_k| + q_k}{2} f_{j,k} + \frac{q_k - |q_k|}{2} f_{j+1,k} \\ &:= \eta^+_{j,k} + \eta^-_{j+1,k}, \end{aligned} \tag{3.9}$$

$$\begin{aligned} \xi_{j,k+\frac{1}{2}} &= \frac{|q_j^* - q_{k+\frac{1}{2}}| + (q_j^* - q_{k+\frac{1}{2}})}{2} f_{j,k} + \frac{(q_j^* - q_{k+\frac{1}{2}}) - |q_j^* - q_{k+\frac{1}{2}}|}{2} f_{j,k+1} \\ &:= \xi^+_{j,k} + \xi^-_{j,k+1}. \end{aligned} \tag{3.10}$$

Here we have used edge-values for the velocity discretization[41] and $q_{k+\frac{1}{2}} = \frac{q_k + q_{k+1}}{2}$. q_j^* is computed using a midpoint rule for the integral (2.4), i.e.

$$q_j^* = \frac{\sum_{i,k} \kappa(|x_j - x_i|) f_{i,k} q_k \Delta x \Delta q}{\sum_{i,k} \kappa(|x_j - x_i|) f_{i,k} \Delta x \Delta q}. \tag{3.11}$$

The extension to high resolution in space is straightforward using a slope limiter. More specifically, denote

$$\eta_{j+\frac{1}{2},k} = \eta^+_{j+\frac{1}{2},k} + \eta^-_{j+\frac{1}{2},k}, \tag{3.12}$$

and let

$$\eta^+_{j+\frac{1}{2},k} = \eta^+_{j,k} + \frac{\Delta x}{2} \sigma^+_{j,k}, \quad \sigma^+_{j,k} = \frac{\eta^+_{j+1,k} - \eta^+_{j,k}}{\Delta x} \varphi\left(\frac{\eta^+_{j,k} - \eta^+_{j-1,k}}{\eta^+_{j+1,k} - \eta^+_{j,k}} \right), \tag{3.13}$$

$$\eta^-_{j+\frac{1}{2},k} = \eta^-_{j+1,k} - \frac{\Delta x}{2} \sigma^-_{j+1,k}, \quad \sigma^-_{j,k} = \frac{\eta^-_{j,k} - \eta^-_{j-1,k}}{\Delta x} \varphi\left(\frac{\eta^-_{j+1,k} - \eta^-_{j,k}}{\eta^-_{j,k} - \eta^-_{j-1,k}} \right). \tag{3.14}$$

Here φ is the slope limiter function such as the Van Leer function[41]:

$$\varphi(\theta) = \frac{|\theta| + \theta}{1 + |\theta|}. \tag{3.15}$$

To construct a second-order scheme in velocity, we add a flux limiter.[42] Then (3.8) is modified to

$$\partial_t f_{j,k} + \frac{\eta_{j+\frac{1}{2},k} - \eta_{j-\frac{1}{2},k}}{\Delta x} + \gamma \frac{\xi_{j,k+\frac{1}{2}} - \xi_{j,k-\frac{1}{2}}}{\Delta q} + \gamma \frac{C_{j,k+\frac{1}{2}} - C_{j,k-\frac{1}{2}}}{\Delta q} = 0. \quad (3.16)$$

Here $C_{j,k+\frac{1}{2}}$ is the corrector defined as

$$C_{j,k+\frac{1}{2}} = \frac{1}{2}|s_{j,k+\frac{1}{2}}| \left(1 - \frac{\Delta t}{\Delta q}|s_{j,k+\frac{1}{2}}|\right) \tilde{W}_{j,k+\frac{1}{2}}, \quad (3.17)$$

where $s_{j,k-\frac{1}{2}} = q_j^* - q_{k-\frac{1}{2}}$, $W_{j,k-\frac{1}{2}} = f_{j,k} - f_{j,k-\frac{1}{2}}$, and $\tilde{W}_{j,k-\frac{1}{2}} = W_{j,k-\frac{1}{2}} \varphi \cdot \left(\frac{W_{j,\mathbf{k}-\frac{1}{2}}}{W_{j,k-\frac{1}{2}}}\right)$. The subscript $\mathbf{k}$ is $k-1$ if $s_{j,k-\frac{1}{2}} > 0$ and $k+1$ if $s_{j,k-\frac{1}{2}} < 0$. φ is again the Van Leer function (3.15).

For the continuum system (2.9), we use a kinetic vector splitting method.[23,48,31] In particular, denote $\rho_j = \rho(t, x_j)$, $\tilde{q}_j = q(t, x_j)$, we have the following semi-discrete scheme for macroscopic system:

$$\partial_t U_j + \frac{F_{j+\frac{1}{2}} - F_{j-\frac{1}{2}}}{\Delta x} = S_j, \quad (3.18)$$

where

$$U_j = \int (1, q)^T f(t, x_j, q) dq := (\rho_j, \rho_j \tilde{q}_j)^T, \quad (3.19)$$

$$\begin{aligned} F_{j+\frac{1}{2}} &= \int (1, q)^T \frac{q + |q|}{2} \rho_j \delta(q - \tilde{q}_j) dq + \int (1, q)^T \frac{q - |q|}{2} \rho_{j+1} \delta(q - \tilde{q}_{j+1}) dq \\ &= \left(\frac{\tilde{q}_j + |\tilde{q}_j|}{2} \rho_j + \frac{\tilde{q}_{j+1} - |\tilde{q}_{j+1}|}{2} \rho_{j+1}, \right. \\ &\quad \left. \tilde{q}_j \frac{\tilde{q}_j + |\tilde{q}_j|}{2} \rho_j + \tilde{q}_{j+1} \frac{\tilde{q}_{j+1} - |\tilde{q}|_{j+1}}{2} \rho_{j+1} \right)^T, \end{aligned} \quad (3.20)$$

$$S_j = (0, \gamma \rho_j (q_j^* - \tilde{q}_j))^T. \quad (3.21)$$

Now let us denote

$$F_j^+ = \left(\frac{\tilde{q}_j + |\tilde{q}_j|}{2} \rho_j, \frac{\tilde{q}_j + |\tilde{q}_j|}{2} \rho_j \tilde{q}_j \right)^T, \quad F_j^- = \left(\frac{\tilde{q}_j - |\tilde{q}_j|}{2} \rho_j, \frac{\tilde{q}_j - |\tilde{q}_j|}{2} \rho_j \tilde{q}_j \right)^T, \quad (3.22)$$

then the fluxes in (3.20) are $F_{j+\frac{1}{2}} = F_j^+ + F_{j+1}^-$. A second-order extension of the fluxes can be computed as follows. Write $F_{j+\frac{1}{2}} = F_{j+\frac{1}{2}}^+ + F_{j+\frac{1}{2}}^-$, and define $F_{j+\frac{1}{2}}^{\pm}$ in

the same manner as that in (3.13), (3.14). That is,

$$F^+_{j+\frac{1}{2}} = F^+_j + \frac{\Delta x}{2}\sigma^+_j, \quad \sigma^+_j = \frac{F^+_{j+1} - F^+_j}{\Delta x}\varphi\left(\frac{F^+_j - F^+_{j-1}}{F^+_{j+1} - F^+_j}\right), \tag{3.23}$$

$$F^-_{j+\frac{1}{2}} = F^-_{j+1} - \frac{\Delta x}{2}\sigma^-_{j+1}, \quad \sigma^-_j = \frac{F^-_j - F^-_{j-1}}{\Delta x}\varphi\left(\frac{F^-_{j+1} - F^-_j}{F^-_j - F^-_{j-1}}\right). \tag{3.24}$$

3.3. *Interface condition*

This section is concerned with the connection between two cells of different types. Let J be the position that separates two regimes such that all $j < J$ belong to the kinetic regime and $j \geq J$ are in the continuum regime. Then we propose the following interface condition.

- To compute $f_{J-1,k}$ via (3.8), we need to prescribe $f_{J,k}$ at the last time step. Since $f_{J,k}$ falls into the continuum regime, this can be done simply by using the *local equilibrium*. Namely

$$f_{J,k}(q) = \rho_J \delta(q_k - \tilde{q}_J). \tag{3.25}$$

- To compute ρ_J and $\tilde{q}_J$ via (3.18), we need ρ_{J-1} and $\tilde{q}_{J-1}$ from the last step. This is done by taking the moments of f_{J-1} thanks to the relationship (1.3). More precisely, we have

$$\rho_{J-1} = \sum_k f_{J-1,k}\Delta q, \quad \rho_{J-1}\tilde{q}_{J-1} = \sum_k f_{J-1,k} q_k \Delta q. \tag{3.26}$$

Remark 3.2. This simple choice of interface condition is inspired by the observation that density and macroscopic velocity should undergo a *continuous* transition as γ remains unchanged between these two regimes. Similar conditions have been used in Ref. 27 for rarefied gas dynamics. However, if we want to deal with the cases when γ has a *discontinuous* or *sharp* transition in magnitude, different interface conditions may need to be used to take into account the possible *boundary layer*, and this is beyond the scope of the current paper.

Now the fully discrete algorithm is in order. Denote $f^n_{j,k} = f(t^n, x_j, q_k)$, $\rho^n_j = \rho(t^n, x_j)$, $\tilde{q}^n_j = \tilde{q}(t^n, x_j)$, $q^{*,n}_j = q^*(t^n, x_j)$. At time t^n, also denote by C^n the collection of cells that are in the continuum regime, i.e. $[x_{j-\frac{1}{2}}, x_{j+\frac{1}{2}}]_{j\in C^n}$ is in continuum regime, and by K^n the collection of cells in the kinetic regime, where $C^n \cup K^n = X = \{1, 2, \ldots, N_x\}$. We have $(\rho^n_j, \tilde{q}^n_j)$ for $j \in C^n$, and f^n_j for $j \in K^n$.

- Compute $q^{*,n}_j$ for all j and $\tilde{q}^n_j$, ρ^n_j for $j \in K^n$ via (3.26).
- Find the set K^{n+1} of all j such that $|q^{*,n}_j - \tilde{q}^n_j| > \epsilon_0$ or $\rho^n_j > \rho_{\max}$, which is the new kinetic regimes. Then the new continuum regime is $C^{n+1} = X \backslash K^{n+1}$.
- For $j \in K^{n+1}\backslash K^n$, compute $f^n_{j,k} = \rho^n_j \delta(q_k - \tilde{q}^n_j)$, where δ is approximated using (5.1).

- Calculate $(\rho_j^{n+1}, \tilde{q}_j^{n+1})$ for $j \in C^n$ from (3.18) and use interface condition (3.26) when necessary.
- Calculate $f_{j,k}^{n+1}$ for $j \in K^{n+1}$ from (3.8) and use interface condition (3.25) when necessary.

4. A Level Set Method

As mentioned before, there are cases when the solutions ρ and q_x to the nonlinear system (2.9) blow up in finite time, which implies the formation of shock in q. However, from the underlying microscopic system, these situations happen when the particles' characteristics cross. In other words, the people who are more scared tend to pass through the less scared ones ahead of them, leading to a case where people with different fear levels may be present at the same location. This implies, instead of considering the viscosity shock solution to the system, we should consider the multi-valued solution that is determined by the fear level and corresponding crossing waves. In this section, we develop a level set method that is capable of capturing the multi-valued solution for the continuum system.

Recall the continuum system (2.9):

$$\rho_t + (\rho\tilde{q})_x = 0, \tag{4.1}$$

$$\tilde{q}_t + \tilde{q}\tilde{q}_x = \gamma(q^* - \tilde{q}), \quad q^* = \frac{\int \kappa(|x-y|)\rho(y)\tilde{q}(y)dy}{\int \kappa(|x-y|)\rho(y)dy}. \tag{4.2}$$

Here we use the non-conservative form of the q equation as it produces the same results as the conservative form when there is a classical solution, and generates possible multi-valued solution when classical solution breaks down. First we form a level set function $\Phi(t, x, p)$ such that the multi-valued $\tilde{q}(t, x)$ can be realized as its zero level set, i.e.

$$\Phi(t, x, p) = 0 \quad \text{at } p = \tilde{q}(t, x) \quad \text{or} \quad \Phi(t, x, \tilde{q}(t, x)) \equiv 0. \tag{4.3}$$

The remaining derivation follows that in Refs. 17, 38 and 36. Taking the time derivative of (4.3), one has

$$\partial_t\Phi + \partial_p\Phi\partial_t\tilde{q} = 0,$$

which becomes $\partial_t\Phi + \partial_p\Phi(-\tilde{q}\tilde{q}_x + \gamma(q^* - \tilde{q})) = 0$ thanks to (4.2). Then the level set equation in the phase space follows:

$$\partial_t\Phi + \partial_p\Phi(-pp_x + \gamma(p^* - p)) = 0. \tag{4.4}$$

Taking the spatial derivative of (4.3), one has $\partial_x\Phi + \partial_p\Phi\partial_x\tilde{q} = 0$, thus

$$\partial_x\tilde{q} = -\frac{\partial_x\Phi}{\partial_p\Phi}. \tag{4.5}$$

Plugging (4.5) into (4.4) leads to

$$\partial_t\Phi + p\partial_x\Phi + \gamma\partial_p\Phi(p^* - p) = 0, \tag{4.6}$$

where $p^*(t,x)$ depending on the density will be defined later (see (4.11)). For smooth initial data $\tilde{q}_0(x)$, the initial condition for Φ is

$$\Phi(0,x,p) = p - \tilde{q}_0(x); \tag{4.7}$$

while for discontinuous $\tilde{q}_0(x)$ such as Riemann initial data, $\Phi(0,x,p)$ should be chosen as the signed distance function to the interface $p = \tilde{q}_0(x)$.[38] Now, we need to derive the evolution equation for density ρ. Since $\tilde{q}$ is multi-valued, ρ can be multi-valued too. Denote $\rho(t,x) \equiv \hat{\rho}(t,x,\tilde{q}(t,x))$, as $\rho(t,x)$ solves (4.1), $\hat{\rho}$ satisfies the following equation:

$$\partial_t\hat{\rho} + \hat{\rho}\partial_x\tilde{q} + \tilde{q}\partial_x\hat{\rho} + \partial_p\hat{\rho}(\partial_t\tilde{q} + \tilde{q}\partial_x\tilde{q}) = 0.$$

Then plug (4.5) and (4.2) into the above equation, we have

$$\partial_t\hat{\rho} + p\partial_x\hat{\rho} + \gamma(p^* - p)\partial_p\hat{\rho} = \hat{\rho}\frac{\Phi_x}{\Phi_p}, \tag{4.8}$$

where we have again used $p = \tilde{q}$. Here the drawback of Eq. (4.8) is that Φ_p can be zero, which makes its right-hand side singular. Notice, however, that the physically relevant density should not be multi-valued, so, inspired by Ref. 36, we consider it to be the projection of its value in phase space onto the curve $\Phi = 0$, i.e.

$$\bar{\rho}(t,x) = \int \hat{\rho}(t,x,p)\delta(\Phi(p))|\Phi_p|dp. \tag{4.9}$$

Similarly the total fear is defined as

$$\bar{Q}(t,x) = \int p\hat{\rho}(t,x,p)\delta(\Phi(p))|\Phi_p|dp, \tag{4.10}$$

and thus

$$p^*(t,x) = \frac{\int(\kappa * \hat{\rho})p\delta(\Phi(p))|\Phi_p|dp}{\int(\kappa * \hat{\rho})\delta(\Phi(p))|\Phi_p|dp}. \tag{4.11}$$

Now, we define a new quantity

$$g(t,x,p) = \hat{\rho}(t,x,p)|\Phi_p(t,x,p)|. \tag{4.12}$$

As always, we need to write down the evolution equation for g. To this end, taking the derivative of (4.6) with respect to p, we obtain the following equation for Φ_p:

$$\partial_t\Phi_p + p\partial_x\Phi_p + \gamma(p^* - p)\partial_p\Phi_p = -\Phi_x + \gamma\Phi_p. \tag{4.13}$$

Then g defined in (4.12) solves

$$\begin{aligned}
&\partial_t g + p\partial_x g + \gamma(p^* - p)\partial_p g \\
&\quad = |\Phi_p|(\partial_t\hat{\rho} + p\partial_x\hat{\rho} + \gamma(p^* - p)\partial_p\hat{\rho}) + \hat{\rho}(\partial_t|\Phi_p| + p\partial_x|\Phi_p| + \gamma(p^* - p)\partial_p|\Phi_p|) \\
&\quad = \hat{\rho}\frac{\Phi_x}{\Phi_p}|\Phi_p| + \hat{\rho}(-\Phi_x + \gamma\Phi_p)\,\mathrm{sgn}(\Phi_p) \\
&\quad = \gamma\hat{\rho}|\Phi_p| = \gamma g,
\end{aligned} \tag{4.14}$$

where the second equality uses (4.8) and (4.13). The initial condition for g reads as follows:

$$g(0,x,p) = \rho_0(x)|\Phi_p(0,x,p)|, \tag{4.15}$$

and if $\Phi(0,x,p)$ takes the form (4.7), then $g(0,x,p) = \rho_0(x)$.

To summarize, one can solve (4.6) and (4.14) with initial conditions (4.7) and (4.15), respectively. Then $\tilde{q}$ takes the zero level set of $\Phi(t,x,p)$, and $\bar{\rho}(t,x)$ and $\bar{Q}(t,x)$ are computed via

$$\bar{\rho}(t,x) = \int g(t,x,p)\delta(\Phi(p))dp, \quad \bar{Q}(t,x) = \int pg(t,x,p)\delta(\Phi(p))dp. \tag{4.16}$$

Remark 4.1. It is interesting to point out that g solves the same equation as the kinetic probability density f, which suggests some similarity between the kinetic formulation and level set formulation, as both of them lift the dimension of the problem by one and unfold the multiple values. In fact, this relation has been observed in the literature of computing multi-valued physical observables for geometrical optics, such as Refs. 36, 26 and 35. The advantage of the level set approach is that the high dimensionality from the phase space can be compensated for by using the local level set method (consult e.g. Ref. 47), which reduces the computational complexity to that comparable to a computation in the physical space. By contrast, the kinetic formulation is amenable to the hybrid construction in Sec. 3 thanks to its close relation with the macroscopic quantities.

5. Numerical Examples

We present several examples to validate our hybrid scheme and level set method in this section. In what follows, we always take $q \in [L_{q1}, L_{q2}]$ with $L_{q1} = 0$, $L_{q2} = 3$ and $x \in [L_{x1}, L_{x2}]$ with $L_{x1} = -50$, $L_{x2} = 50$. Again N_q and N_x denote the number of points in q- and x-directions, respectively. We assume Neumann boundary conditions in both q and x. The time step Δt is chosen to satisfy the CFL condition. For the continuum system, the time step is $\Delta t = \frac{\Delta x}{\max(q_I)}$ where q_I is the initial velocity; for kinetic equation, hybrid scheme and level set method, the time step is all chosen as $\Delta t = \frac{1}{2}\min\{\frac{\Delta x}{q_{\max}}, \frac{\Delta q}{2q_{\max}\gamma}\}$; here $q_{\max} = \max_j q_j$.

The delta function in the kinetic and hybrid scheme is approximated by

$$\delta(q) \sim E(q) = \frac{1}{\sqrt{\pi}R_0} e^{-\frac{q^2}{R_0^2}}, \quad R_0 = 0.04 \tag{5.1}$$

when necessary, and Δq is small enough to resolve it. The interaction kernel we choose here takes the form

$$K(x) = \frac{1}{x^2 + R^2}\frac{R}{\pi}. \tag{5.2}$$

For the level set method, Eqs. (4.6) and (4.14) are discretized similarly to the kinetic equation, and the delta function in computing the moments (4.16) takes the

following approximation[36]:

$$\delta_\eta(K(t,x,p)) = \begin{cases} \dfrac{1}{2\eta}\left(1+\cos\dfrac{|\pi K(t,x,p)|}{\eta}\right), & |K(t,x,p)| \le \eta(t,x), \\ 0, & |K(t,x,p)| > \eta(t,x), \end{cases} \tag{5.3}$$

where $\eta(t,x) = 2\max_p(|\phi_p(t,x,p)|,1)\Delta p$. Here $p \in [L_{q1}, L_{q2}]$ with $L_{q1} = 0$, $L_{q2} = 3$.

5.1. *Asymptotic property*

We first check the asymptotic behavior of the solution in the spatially homogeneous case. Consider equation $f_t = \gamma[(q-q^*)f]_q$ with *non-equilibrium* initial data $f(0,q) = \frac{3}{4}E(q-0.6) + \frac{1}{4}E(q-1.2)$ and a fixed $q^* = 1$. Δq is chosen 0.02 to resolve the δ function in (5.1). The first three figures in Fig. 1 display the evolution of $f(t,q)$ toward a local equilibrium. We start with a non-equilibrium initial data and as times goes on f concentrates on q^*. Figure 1 on the bottom right presents the distance $|\tilde{q}(t) - q^*|$ in time with $\gamma = 1$, 2 and 3 respectively, where we see that bigger γ gives faster convergence rate as implied in the proof of Proposition 3.1.

Next we consider the spatially inhomogeneous case $f_t + qf_x = \gamma((q-q^*)f)_q$ with $\gamma = 100$ and initial data

$$\begin{aligned} &\rho_I(0,x) = \sin\left(\frac{\pi x}{10}\right) + 2, \quad q_I(0,x) = \frac{1}{2}(3-\tanh x), \\ &f_I(x,q) = \rho_I(x)\left(\frac{1}{4}E(q-q_I(x)-0.5) + \frac{3}{4}E(q-q_I(x)+0.3)\right). \end{aligned} \tag{5.4}$$

Figure 2 shows the evolution of $f(t,x,q)$. Initially $f_I(x,q)$ has two bumps in q for every x, as displayed in the left plot of Fig. 2. As time evolves, $f(t,x,q)$ starts to concentrate on $\tilde{q}(t,x)$, as confirmed by the right plot of Fig. 2 where the projection of f onto the (x,q)-plane matches well with $\tilde{q}(t,x)$.

5.2. *Convergence test*

In this section, we perform a convergence test to check that the interface condition proposed in Sec. 3.3 will not violate the accuracy of the scheme. Consider the spatially inhomogeneous case with smoothed Riemann initial data

$$\rho_I(x) \equiv 1, \quad q_I(x) = \frac{1}{2}(3-\tanh(0.25x)), \quad f_I(x,q) = \rho_I(x)E(q-q_I(x)). \tag{5.5}$$

We fix $\Delta q = 0.001$, and take the space mesh size $\Delta x = \frac{1}{10}, \frac{1}{20}, \frac{1}{40}, \frac{1}{80}, \frac{1}{160}$, respectively. $q_{\max} = \max_j\{q_j\}$. The output time is $t_{\max} = 0.1$, and we check the error in l^1-norm at $t = t_{\max}$,

$$\operatorname*{error}_{\Delta x} = \|\xi_{\Delta x}(t_{\max}) - \xi_{2\Delta x}(t_{\max})\|_{l^1}, \tag{5.6}$$

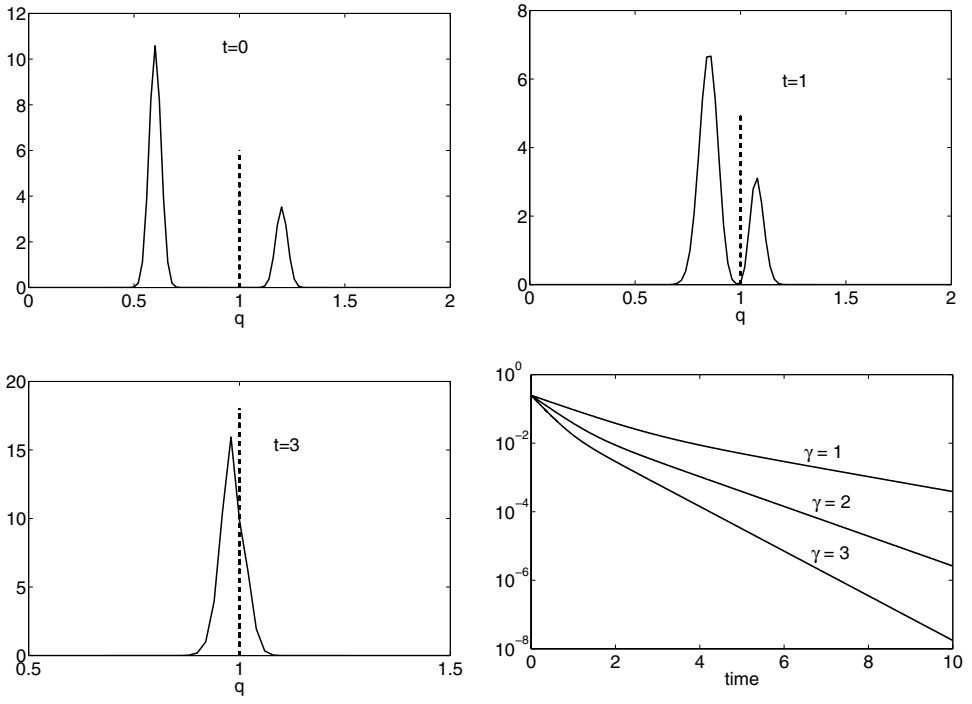

Fig. 1. Solution to the spatially homogeneous equation (3.1) with non-equilibrium initial data (see the upper left figure). The next two figures display the solution with time $t = 1$ and 3, respectively. The dotted line in these three figures denotes q^*. The lower right plots the distance $|\tilde{q}(t) - q^*|$ vs. time for $\gamma = 1$, 2 and 3.

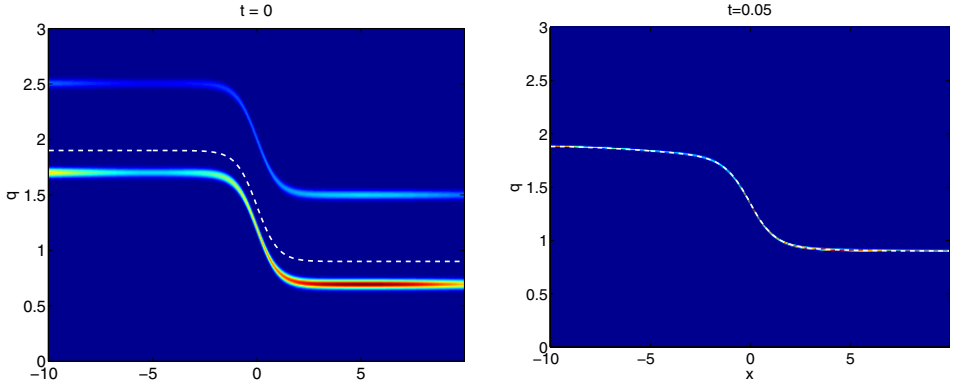

Fig. 2. Plot of $f(t, x, q)$ to the space inhomogeneous equation with initial data (5.4). Left: initial configuration. Right: plot at time $t = 0.05$. Overlaid with the plot of macroscopic bulk fear $\tilde{q}(t, x)$ (dashed white line) at initial and final times.

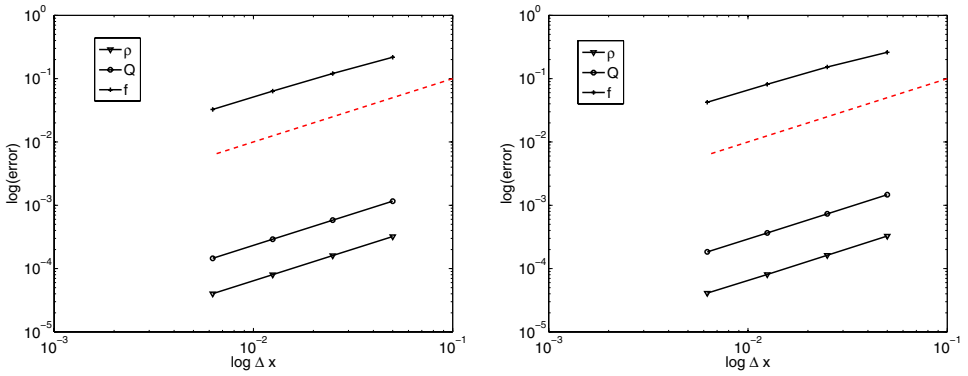

Fig. 3. (Color online) Plot of relative error (5.6) vs. mesh size Δx. Here $x \in [-50, 50]$, $q \in [0, 3]$. Left: kinetic equation. Right: hybrid scheme with $\rho_{\max} = 1.01$, $\epsilon_0 = \max_x |q(\tilde{0}, x) - q^*(0, x)|$. The red dashed curves have slope 1.

where ξ can be f, ρ and Q. The equilibration rate is $\gamma = 0.1$ and interaction radius is $R = 0.1$. We only check hybrid scheme with first-order discretization (3.8)–(3.10) and (3.18)–(3.21). The results are collected in Fig. 3, where a uniform first-order accuracy is observed.

5.3. *Riemann problem*

In this section, we compare our hybrid scheme and level set method with the solutions to the kinetic and continuum systems for relatively long times after the crossing of characteristics. Here the initial density takes the form

$$\rho_I(x) = \frac{\rho_L}{2}(1 - \tanh(20x)) + \frac{\rho_R}{2}(1 + \tanh(20x)), \tag{5.7}$$

with $\rho_L = 2$ and $\rho_R = 1$, and initial fear is chosen as

$$q_I(x) = \frac{1}{2}(3 - \tanh(x)). \tag{5.8}$$

The equilibrium rate is $\gamma = 0.1$, and $R = 0.1$ in the interaction kernel (5.2). Our meshes are $\Delta x = 0.05$, $\Delta q = \Delta p = 0.01$. We use a moving frame with velocity $s = \frac{\sqrt{\rho_L} q_L + \sqrt{\rho_R} q_R}{\sqrt{\rho_L} + \sqrt{\rho_R}} = 1.5858$ (the formula for the shock speed obtained in Ref. 7). The results are gathered in Fig. 4, where we compare the density $\rho(t, x)$, multi-valued velocity $\tilde{q}(t, x)$, and averaged velocity $\frac{Q(t,x)}{\rho(t,x)}$. For the continuum system, it immediately gives $\tilde{q}\rho = Q$, while for the kinetic equation and level set formulation, the density $\rho(t, x)$ and total fear $Q(t, x)$ are calculated via (1.3) and (4.16), respectively. Here, a good agreement is observed among the kinetic system, hybrid scheme, and level set method, while the continuum system fails to capture the detailed dynamics in the vicinity of the shock.

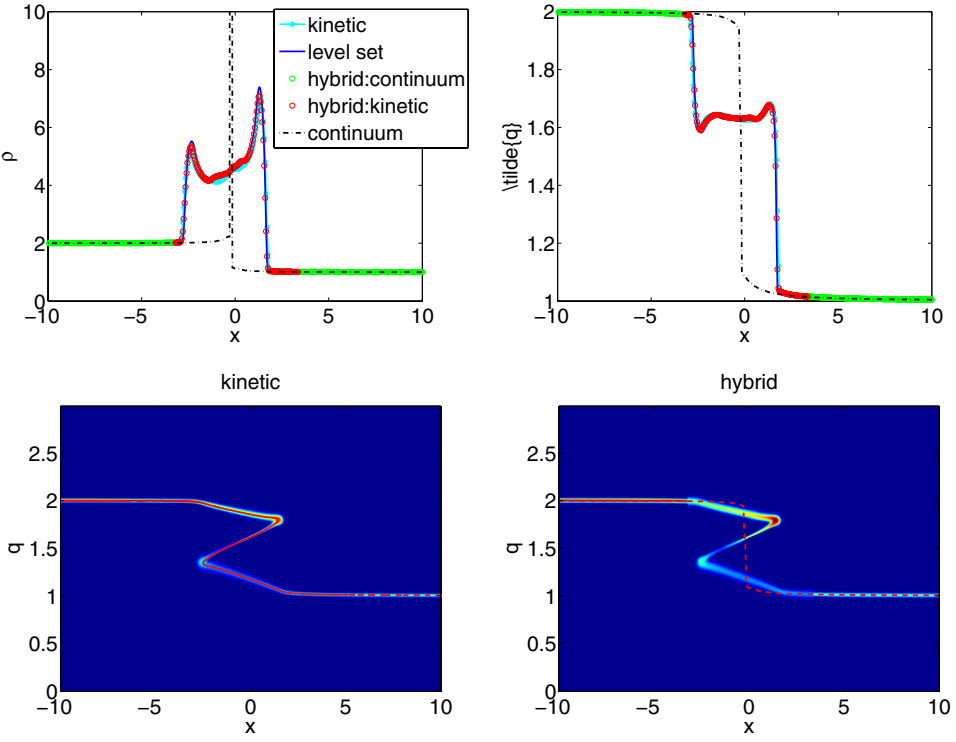

Fig. 4. (Color online) Solution to the kinetic model and continuum system with Riemann initial data (5.5), (5.7). Upper left: plot of macroscopic density $\rho(t,x)$. Upper right: plot of macroscopic fear $\tilde{q}(t,x)$. Lower left: plot of the solution $f(t,x,q)$ to the kinetic equation, overlaid with the contour plot of the zero level set of $\Phi(t,x)$. Lower right: plot of $f(t,x,q)$ using the hybrid scheme, and the red dashed curve is $\tilde{q}(x)$ in the continuum model. Here $\gamma = 0.1$, $R = 0.1$, and final time is $t = 10$. For the hybrid scheme, we choose $\rho_{\max} = 2.1$ and $\epsilon_0 = 0.0489$ from (3.6).

To better confirm that our hybrid scheme is able to detect different regimes automatically, we consider the following initial condition:

$$\rho_I(x) = \frac{\rho_L}{2}(1 - \tanh(20(x-10))) + \frac{\rho_R}{2}(1 + \tanh(20(x-10))), \tag{5.9}$$

$$q_I(x) = \frac{1}{2}(2.6 - 0.8\tanh(x+10) - 0.6\tanh(x-10)) \tag{5.10}$$

with $\rho_L = 2$ and $\rho_R = 1$, which will produce a two-shock solution. Again the parameters are as follows: $\gamma = 0.1$, $R = 0.1$, final time $t = 10$, and for the hybrid scheme, $\rho_{\max} = 2.1$ and $\epsilon_0 = 0.0299$ from (3.6). Additionally, we use a moving mesh with speed $s = 1.6$, which is the speed for the left shock. With exactly the same grid, one sees in Fig. 5 that the solution from the continuum model is inferior to the hybrid scheme or level set method, both of which are in good match with the solution to the kinetic equation.

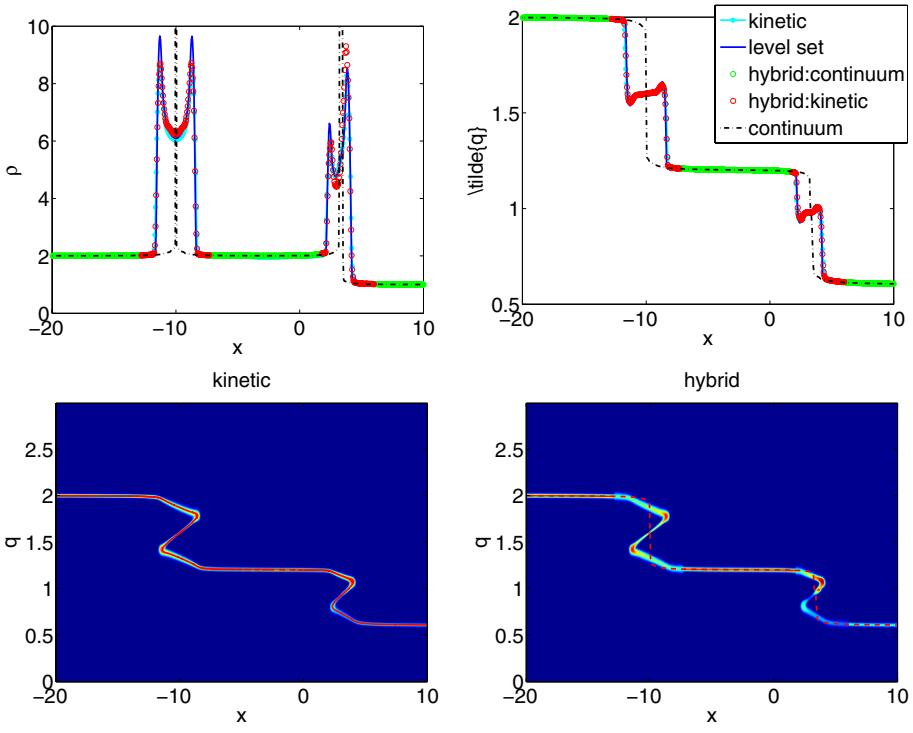

Fig. 5. (Color online) Solution to the Riemann initial data (5.9), (5.10) using the kinetic model, continuum model, hybrid scheme, and level set method. Upper left: plot of macroscopic density $\rho(t,x)$. Upper right: plot of macroscopic fear $\tilde{q}(t,x) = \frac{Q(t,x)}{\rho(t,x)}$. Lower left: the solution $f(t,x,q)$ to the kinetic equation, overlaid with the contour zero of the level set method. Lower right: plot of $f(t,x,q)$ using the hybrid scheme, with the red dashed curve being $\tilde{q}(x)$ in the continuum model.

5.4. *General initial data*

In this section, we consider a more general initial data which mimics a one-dimensional version of the crowd motion in a traditional hajj pilgrimage. The initial density and emotion level take the following form:

$$\rho_I(x) = 0.5e^{-2(x-1)^2} + 0.5e^{-2(x+1)^2} + 0.1 - 0.1e^{-x^2}, \tag{5.11}$$

$$q_I(x) = 1.1 - e^{-x^2/2}, \tag{5.12}$$

and their plots are displayed in the upper left of Fig. 6. Here the region around the origin represents the pillar at which stoning of the devil ritual takes place, therefore the density has two bumps around it. The emotional level here represents people's willing to move forward, so people who are around the pillar tend to stay put and thus cause a well in q_I around this region. The other parameters are $\gamma = 0.1$ and $R = 0.1$, and final time is $t = 5$. For hybrid scheme, we choose $\rho_{\max} = \max_x \rho_I(x) = 0.5644$. Solutions are plotted in Fig. 6, where one sees that there are two peaks in density, showing that these two places are the more dangerous to have

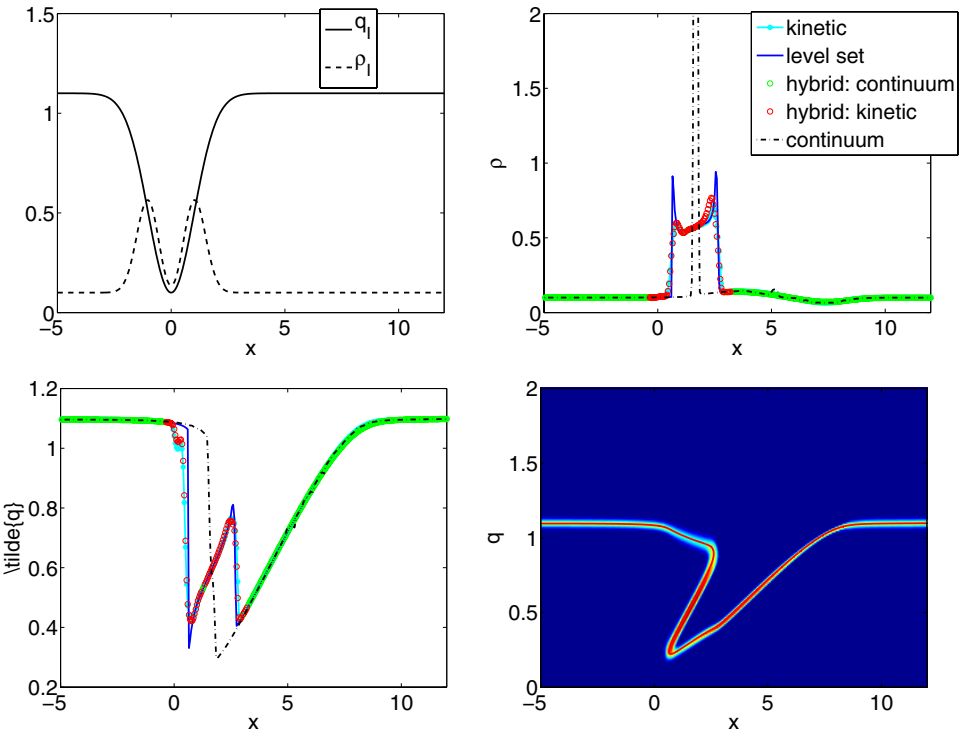

Fig. 6. Upper left: plot of the initial data (5.11), (5.12). Rest three are solutions at time $t = 5$ using kinetic model, continuum system, hybrid scheme and level set method. Upper right: macroscopic density $\rho(t, x)$. Lower left: bulk fear level $\tilde{q}(t, x)$. Lower right: $f(t, x, q)$ to the kinetic equation, overlaid with the contour zero of the level set method.

crowd stampede. The multiple values in q in the lower right figure correspond to the fact that around the pillar, there are people with different emotions — a portion of them want to stay and others want to move forward. Recall the recent tragedy of stampede near the holy city of Mecca, where a more detailed two-dimensional modeling and simulation are expected, which we discuss below.

6. Future Work

In this paper, we have heavily explored the one-dimensional crowd model analyzed in Ref. 7. While certain real-world scenarios may in fact be pseudo-one-dimensional — long, narrow hallways for example — a two-dimensional model would likely be more appropriate for most scenarios. Though fully developing such a model is outside the scope of this paper, we can offer some ideas as to what form such a model might take, as well as how one might approach domain decomposition of the type performed here within such a model.

Harkening back to the discrete model presented in (2.1), it is assumed there that all of the agents wish to move in the positive x-direction. However, one could

easily generalize by simply modeling the velocity of agent i as having magnitude q_i, but having a direction $\hat{a}_i(t)$ that may vary from person-to-person and from moment-to-moment:

$$\frac{d\mathbf{x}_i}{dt} = q_i \hat{a}_i. \tag{6.1}$$

This would retain the original model's idea that fear directly affects how quickly the agents move, but would now allow the pedestrians to at least attempt some sort of path planning through varying directions.

To complete such a model, one would have to specify how $\hat{a}_i(t)$ is chosen or evolves. Here there are many possibilities. One method might generally fall under the category of behavioral heuristics. Imagine, for example, that the panicking agents have two potentially competing goals: (1) to move as directly as possible toward a specific point in space that is presumably deemed safe (an exit, shelter, etc.) and (2) to avoid running into obstacles and other pedestrians as much as possible along the way. One could presumably construct a sort of energy function for the pedestrians that would include these two factors, such that the minimum of this energy would correspond the direction that achieves the best balance. Agents could then make short time horizon optimization choices as they move through the crowd, discretely choosing new directions on occasion, or could instead continuously move down gradients of this energy as they travel. In fact, a model along these lines is presented in Ref. 22, though this work does not consider the role of fear or contagion.

Given a discrete model along these lines, one could likely formulate both macroscopic and kinetic versions. Under the monokinetic assumption, the PDE representation would introduce another equation for the quantity $\hat{a}(\mathbf{x}, t)$, which could be algebraic if agents make optimization choices directly, or could itself be a PDE if agents tend to travel down energy gradients continuously. Importantly, though, one would need to assume in this case that all agents at location $\mathbf{x}$ at time t would choose the same direction $\hat{a}(\mathbf{x}, t)$. However, if we relax the monokinetic assumption and move toward a kinetic model, we might instead expand phase space to now include the angle of motion as well, making the phase space four-dimensional, plus time.

In terms of numerics, we would need to consider the new quantity $\hat{a}(\mathbf{x}, t)$ in the same way as q. More precisely, f would depend on time t, space $\mathbf{x}$, and "velocity" $(q, \hat{a})$. The evolution of $\hat{a}(\mathbf{x}, t)$ could be separated from the equation of f or its macroscopic counterpart, and kept the same across different models: agent-based, kinetic, and continuum. Thus it should not be difficult to determine the asymptotic relation between the kinetic and macroscopic models as one can always do this by considering the spatially homogeneous scenario. As a result, a similar regime indicator to that used in this work would follow. To implement a hybrid scheme in higher-space dimension, we could simply use a Cartesian grid and extend the one-dimensional method using a dimension-by-dimension technique. A more elaborated

method would use adaptive mesh or immersed interface methods. Likewise, the level set method that we derived in one-dimensional can be seamlessly generalized to higher dimensions, as one only needs to re-derive the level set equation using a vector form. Nevertheless, special treatment would be needed to preserve the norm of $\hat{a}(\mathbf{x}, t)$.

7. Conclusions

We constructed two numerical schemes for crowd dynamics with emotional contagion. Here the kinetic description provides better resolution than the macroscopic model whose viscosity solution becomes incorrect when the characteristics at the particle level cross. However, because of the high dimensionality, solving the kinetic equation is often expensive and sometimes unnecessary. Our first approach is a hybrid method that connects a continuum solver with a kinetic solver. The criteria that distinguishes two regimes is based on the macroscopic density and average fear level. The interface condition is proposed according to the continuity of the macroscopic quantities. Unlike previous research on hybrid schemes for kinetic and related problems, which focus on the Boltzmann-type equation with a regular distribution (Maxwellian) as an equilibrium, our method here provides a new way to treat the singular (delta-like) equilibrium. As such types of equilibrium emerge in many other contexts such as biological swarming and opinion dynamics, it is desirable to apply our method to a broader scope. Our second approach is in the level set framework, which is inspired by the observation that the crossing of characteristics for particles results in a multi-valued solution in the fear for the continuum system. Although the so-derived level set equations live in a higher dimension than the macroscopic system, they can be solved just around the zero level set, which reduces the computational cost to that comparable to the macroscopic solver. Future research would be on deriving a more systematic expansion of the solution so that we can perform high-order coupling. Rigorous convergence toward the monokinetic distribution as well as the convergence rate is still lacking and would be an interesting project.

Acknowledgments

This work is funded by ARO MURI Grant W911NF-11-1-0332 and NSF Grant CMMI-1435709 and DMS-1620135.

References

1. D. Amadori and M. DiFrancesco, The one-dimensional Hughes model for pedestrian flow: Riemann-type solutions, *Acta Math. Sci. Ser. B Engl. Ed.* **32** (2012) 259–280.
2. C. Appert-Rolland, P. Degond and S. Motsch, Two-way multi-lane traffic model for pedestrians in corridors, *Netw. Heterog. Media* **6** (2011) 351–381.
3. G. Bal and Y. Maday, Coupling of transport and diffusion models in linear transport theory, *Math. Model. Numer. Anal.* **36** (2002) 69–86.
4. N. Bellomo, A. Bellouquid and D. Knopoff, From the microscale to collective crowd dynamics, *Multiscale Model. Simulat.* **11** (2013) 943–963.

5. N. Bellomo and C. Dogbe, On the modeling of traffic and crowds: A survey of models, speculations and perspectives, *SIAM Rev.* **53** (2011) 409–463.
6. N. Bellomo and L. Gibelli, Toward a mathematical theory of behavior-social dynamics for pedestrian crowds, *Math. Models Methods Appl. Sci.* **25** (2015) 2417–2437.
7. A. Bertozzi, J. Rosado, M. Short and L. Wang, Contagion shocks in one dimension, *J. Stat. Phys.* **158** (2014) 647–664.
8. T. Bosse, R. Duell, Z. A. Memon, J. Treur and C. N. V. D. Wal, A multi-agent model for mutual absorption of emotions, in *European Council on Modeling and Simulation ECMS* **2009** (2009) 212–218.
9. F. Bouchut, On zero pressure gas dynamics, *Ser. Adv. Math. Appl. Sci.* **22** (1994) 171–190.
10. F. Bouchut, S. Jin and X. Li, Numerical approximations of pressureless and isothermal gas dynamics, *SIAM. J. Numer. Anal.* **41** (2004) 135–158.
11. J.-F. Bourgat, P. Le Tallec, B. Perthame and Y. Qiu, Coupling Boltzmann and Euler equations without overlapping, *Contemp. Math.* **157** (1994) 377–398.
12. W. Braun and K. Hepp, The Vlasov dynamics and its fluctuations in the $1/N$ limit of interacting classical particles, *Commun. Math. Phys.* **56** (1977) 125–146.
13. Y. Brenier and E. Grenier, Sticky particles and scalar conservation laws, *SIAM J. Numer. Anal.* **35** (1998) 2317–2328.
14. J. Carrillo, Y. Choi, E. Tadmor and C. Tan, Critical thresholds in 1D Euler equations with nonlocal forces, *Math. Models Methods Appl. Sci.* **26** (2016) 185–206.
15. J. A. Carrillo, M. Fornasier, G. Toscani and F. Vecil, Particle, kinetic and hydrodynamic models of swarming, in *Mathematical Modeling of Collective Behavior in Socio-Economic and Life Sciences* (Birkhäuser, 2010), pp. 297–336.
16. G. Chen and H. Liu, Formation of δ-shocks and vacuum states in the vanishing pressure limit of solutions to the Euler equations for isentropic fluids, *SIAM J. Math. Anal.* **34** (2003) 925–938.
17. L. Cheng, H. Liu and S. Osher, Computational high frequency wave propagation using the level set method, with applications to the semi-classical limit of Schrödinger equations, *Commun. Math. Sci.* **1** (2003) 593–621.
18. A. Chertock and A. Kurganov, Computing multi-valued solutions of pressureless gas dynamics by deterministic particle methods, *Commun. Comput. Phys.* **5** (2009) 565–581.
19. F. Coquel, S. Jin, J. Liu and L. Wang, Well-posedness and singular limit of a semilinear hyperbolic relaxation system with a two-scale discontinuous relaxation rate, *Arch. Ration. Mech. Anal.* **214** (2014) 1051–1084.
20. N. Crouseilles, P. Degond and M. Lemou, Hybrid kinetic/fluid models for non-equilibrium systems, *C. R. Math.* **336** (2003) 359–364.
21. N. Crouseilles, P. Degond and M. Lemou, A hybrid kinetic-fluid model for solving the gas dynamics Boltzmann-BGK equation, *J. Comput. Phys.* **199** (2004) 776–808.
22. P. Degond, C. Appert-Rolland M. Moussad, J. Pettr and G. Theraulaz, A hierarchy of heuristic-based models of crowd dynamics, *J. Stat. Phys.* **152** (2013) 1033–1068.
23. S. Deshpande, Kinetic theory-based new upwind methods for inviscid compressible flows, *AIAA* **86** (1986) 1–11.
24. G. Dimarco and L. Pareschi, Hybrid multiscale methods II. Kinetic equations, *Multiscale Model. Simulat.* **6** (2008) 1169–1197.
25. C. Dogbe, Modeling crowd dynamics by the mean-field limit approach, *Math. Comput. Model.* **52** (2010) 1506–1520.
26. B. Engquist and O. Runborg, Multi-phase computations in geometrical optics, *J. Comput. Appl. Math.* **74** (1995) 175–192.

27. F. Filbet and T. Rey, A hierarchy of hybrid numerical methods for multiscale kinetic equations, *SIAM J. Sci. Comput.* **74** (2015) A1218–A1247.
28. F. Golse, S. Jin and C. Levermore, The convergence of numerical transfer schemes in diffusive regimes I: The discrete-ordinate method, *SIAM J. Numer. Anal.* **36** (1999) 1333–1369.
29. F. Golse, S. Jin and C. Levermore, A domain decomposition analysis for a two-scale linear transport problem, *Math. Model Numer. Anal.* **37** (2003) 869–892.
30. D. Helbing, A mathematical model for the behavior of pedestrians, *Behav. Sci.* **36** (1991) 298–310.
31. J. Hu and S. Jin, On kinetic flux vector splitting schemes for quantum Euler equations, *Kinet. Relat. Models* **4** (2011) 517–530.
32. W. H. Huang, B. R. Fajen, J. R. Fink and W. H. Warren, Visual navigation and obstacle avoidance using a steering potential function, *Robot. Auton. Syst.* **54** (2006) 288–299.
33. F. Huang and Z. Wang, Well-posedness for pressureless flow, *Commun. Math. Phys.* **222** (2001) 117–146.
34. R. L. Hughes, The flow of human crowds, *Ann. Rev. Fluid Mech.* **35** (2003) 169–182.
35. S. Jin and X. Li, Multi-phase computations of the semiclassical limit of the Schrödinger equation and related problems: Whitham vs. Wigner, *Physica D* **182** (2003) 46–85.
36. S. Jin, H. Liu, S. Osher and R. Tsai, Computing multi-valued physical observables for the semiclassical limit of the Schrödinger equation, *J. Comput. Phys.* **205** (2005) 222–241.
37. S. Jin, J. Liu and L. Wang, A domain decomposition method for semilinear hyperbolic systems with two-scale relaxations, *Math. Comput.* **82** (2013) 749–779.
38. S. Jin and S. Osher, A level set method for the computation of multi-valued solutions to quasi-linear hyperbolic PDE's and Hamilton–Jacobi equations, *Commun. Math. Sci.* **1** (2003) 575–591.
39. A. Klar, H. Neunzert and J. Struckmeier, Transition from kinetic theory to macroscopic fluid equations: A problem for domain decomposition and a source for new algorithm, *Transport Theory Statist. Phys.* **29** (2000) 93–106.
40. P. LeTallec and F. Mallinger, Coupling Boltzmann and Navier–Stokes equations by half fluxes, *J. Comput. Phys.* **136** (1997) 51–67.
41. R. J. Leveque, *Numerical Methods for Conservation Laws* (Birkhäuser-Verlag, 1992).
42. R. J. Leveque, *Finite Volume Methods for Hyperbolic Problems* (Cambridge Univ. Press, 2002).
43. J. Li and H. Yang, Delta-shocks as limits of vanishing viscosity for multidimensional zero-pressure gas dynamics, *Quart. Appl. Math.* **59** (2001) 315–342.
44. J. Li and T. Zhang, Generalized Rankine–Hugoniot relations of delta-shocks in solutions of transportation equations, in *Advances in Nonlinear Partial Differential Equations and Related Areas* (World Scientific, 1997).
45. H. Liu and E. Tadmor, Critical threshold in a convolution model for nonlinear conservation laws, *SIAM J. Appl. Math.* **33** (2001) 930–945.
46. S. Motsch and E. Tadmor, A new model for self-organized dynamics and its flocking behavior, *J. Stat. Phys.* **144** (2011) 923–947.
47. D. Peng, B. Merriman, S. Osher, H. Zhao and M. Kang, A PDE-based fast local level set method, *J. Comput. Phys.* **155** (1999) 410–438.
48. R. D. Reitz, One-dimensional compressible gas dynamics calculations using the Boltzmann equation, *J. Comput. Phys.* **42** (1981) 108–123.

49. T. Rey and C. Tan, An exact rescaling velocity method for some kinetic flocking models, *SIAM J. Numer. Anal.* **54** (2016) 641–664.
50. W. Sheng and T. Zhang, *The Riemann Problem for the Transportation Equations in Gas Dynamics*, Memoirs of the American Mathematical Society, Vol. 654 (Amer. Math. Soc., 1999).
51. E. Tadmor and C. Tan, Critical threshold in flocking hydrodynamics with nonlocal alignment, *Proc. Roy. Soc.* **372** (2014) 20130406.
52. C. Tan, A discontinuous Galerkin method on kinetic flocking models, arXiv: 1409.5509, to appear in *Math. Models Methods Appl. Sci.*
53. M. Tidriri, New models for the solution of intermediate regimes in transport theory and radiative transfer: Existence theory, positivity, asymptotic analysis and applications, *J. Stat. Phys.* **104** (2001) 291–325.
54. J. Tsai, E. Bowring, S. Marsella and M. Tambe, Empirical evaluation of computational emotional contagion models, in *Proc. 10th Int. Conf. Intelligent Virtual Agents*, *IVA'11* (Springer-Verlag, 2011), pp. 384–397.
55. J. Tsai, N. Fridman, E. Bowring, M. Brown, S. Epstein, G. Kaminka, S. Marsella, A. Ogden, I. Rika, A. Sheel, M. E. Taylor, X. Wang, A. Zilka and M. Tambe, Escapes: Evacuation simulation with children, authorities, parents, emotions, and social comparison, in *The 10th Int. Conf. Autonomous Agents and Multiagent Systems*, *AAMAS'11*, Vol. 2 (International Foundation for Autonomous Agents and Multiagent Systems, 2011), pp. 457–464.